DOI 10.1021/acs.jpcc.6b05465

THE JOURNAL OF PHYSICAL CHEMISTRY C

Article

pubs.acs.org/JPCC

Water Affinity and Surface Charging at the z-Cut and y-Cut $LiNbO_3$ Surfaces: An Ambient Pressure X-ray Photoelectron Spectroscopy Study

Kumara Cordero-Edwards,[†] Laura Rodríguez,[†] Annalisa Calò,[†] Ma José Esplandiu,[†] Virginia Pérez-Dieste,[‡] Carlos Escudero,[‡] Neus Domingo,*[,†] and Albert Verdaguer[†,*]

[†]Catalan Institute of Nanoscience and Nanotechnology (ICN2), CSIC and The Barcelona Institute of Science and Technology, Campus UAB, Bellaterra, 08193 Barcelona, Spain

[‡]ALBA Synchrotron Light Source, Carrer de la Llum 2−26, 08290 Cerdanyola del Vallès,Barcelona, Spain

Supporting Information

ABSTRACT: Polarization dependence of water adsorption and desorption on $LiNbO_3$ surfaces was demonstrated using X-ray photoelectron spectroscopy (XPS) carried out in situ under near-ambient conditions. Positive and negative (0001) faces (z-cut) of the same crystal were compared for the same temperature and pressure conditions. Our results indicate a preferential adsorption on the positive face of the crystal with increasing water pressure and also higher desorption temperature of the adsorbed molecular water at the positive face. Adsorption measurements on the $(1\bar{1}00)$ face (y-cut) showed also strong affinity to water, as observed for the z-cut positive surface. We found a direct relation between the capacity of the surface to discharge and/or to screen surface charges and the affinity for water of each face. XPS spectra indicate the presence of OH groups at the surface for all the conditions and surfaces measured.

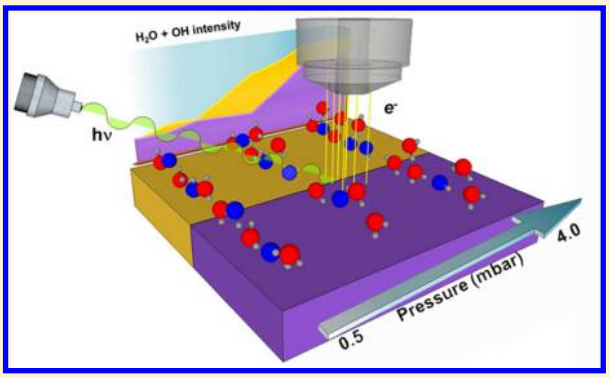

1. INTRODUCTION

Ferroelectric materials are polar materials with a permanent electric dipole below a certain transition temperature. This polarization can be controlled and switched by externally applied electric fields, as it is done in thin-film ferroelectric memories.[1] At the surface of ferroelectric materials, polarization suffers from serious fundamental and practical challenges such as depolarization fields and surface charge screening. Uncompensated surface charges due to the discontinuity of the normal polarization component result in depolarization fields that strongly affect polarization states. The ultimate stability of ferroelectric phases is determined by a balance between bulk thermodynamics and the screening mechanisms for polarization, which can be internal (domain formation or charge carriers migration within the bulk) or external (chemical environment or adsorbates). Moreover, external screening mechanisms are highly dependent on the polarization direction and can even induce permanent changes on the surfaces that persist after polarization switching or removal. Understanding the interplay between ferroelectric phase stability, screening, and atomistic processes at the surface is key to control low-dimensional ferroelectricity.

Several reports devoted to ferroelectric surfaces exposed to ambient conditions show strong experimental evidence for polarization-induced surface charge compensation by ionic adsorption.[2−4] The interplay between polarization and surface adsorbates works in both directions: adsorbates influence polarization, but the orientation of the polarization also determines the type of adsorbates that bond at the surfaces, and it has been demonstrated that ferroelectric surfaces with opposite polarity can have different behavior toward molecules adsorption.[5,6]

$LiNbO_3$ (LN) is a ferroelectric oxide widely used in nonlinear optics and acoustic applications, mainly due to the bulk properties of the material. While these bulk properties are well established, surface properties, and specially the interface with other media, are much less known despite its (0001) ferroelectric surface, also referred to as z-cut, has shown promising applications as chemical sensor.[5,6] Most of the studies to understand the LN z-cut interface have been mainly restricted to vacuum and aqueous solutions, while the interfaces in ambient conditions are still poorly understood. This lack of information mainly arises from the fact that, in the ferroelectric phase, the z-cut surfaces are highly polar, making the experimental study of the surface very challenging because of strong perturbative charging effects. These effects hinder for example the use of scanning tunneling microscopy (STM) or diffraction techniques. Unscreened surface charge also inter-

Received: May 31, 2016
Revised: October 2, 2016

DOI: 10.1021/acs.jpcc.6b05465
J. Phys. Chem. C XXXX, XXX, XXX−XXX

feres with high-resolution atomic force microscopy (AFM) measurements under ambient conditions, and atomic-resolution images have only been obtained in aqueous solution to compensate surface charge.[7]

In this work, the interfaces of positive and negative LN z-cut surfaces at different temperature and water pressure conditions were studied using ambient pressure XPS (AP-XPS). In addition to the LN z-cut surfaces, other measurements were also carried out on the $(1\bar{1}00)$ LN surface, commonly referred as nominally nonpolar y-cut and on a periodically poled lithium niobate (PPLN) crystal. The LN y-cut surface is also of technological relevance[8] and has been considered of special interest because, while being a nonpolar surface from the crystallographic point of view, it shows surface charging[9] and piezoelectricity in the *y* axis.[10] Finally, PPLN, LN z-cut single crystals patterned with alternatively micron wide poled stripes of positive (pointing up) and negative (pointing down) ferroelectric domains, was also tested, since it is widely used as a reference sample in piezoresponse force microscopy (PFM)[11] and optical devices.[12]

Available experimental[6,13,14] and theoretical[15,16] studies point out that the interaction of the LN surface with adsorbates strongly depends on its polarization when polar molecules are involved. Using AP-XPS we were able to study the absorption and desorption of water at pressures up to 5 mbar and temperatures up to 400 °C. We observed polarization-dependent water adsorption and desorption processes and surface discharge dynamics. Our results also demonstrate the presence of OH groups at all LN surfaces explored, although the mechanism of formation of these groups at the surface could not be univocally established.

2. EXPERIMENTAL SECTION

2.1. Sample Preparation and Characterization. Optical grade 10 × 10 × 0.5 mm LN crystals were obtained from MTI Corporation, both in z-cut and y-cut crystalline structure. The z-cut single crystal was cut in two pieces in order to study two areas with opposite polarization. A 3 × 3 × 0.5 mm PPLN crystal was purchased from Asylum Research, Santa Barbara, CA. First, a chemical cleaning treatment was applied to all crystals. The crystals were sonicated for 10 min sequentially in acetone, isopropyl alcohol, and Milli-Q water. Finally, LN single crystals polarization direction was checked by PFM using an MFP-3D AFM (Asylum Research, Santa Barbara, CA). Two different surfaces were studied: the one corresponding to the polarization pointing up (LN z-cut positive surface) and the one corresponding to the polarization pointing down (LN z-cut negative surface), as determined from the phase lag of PFM signal.

2.2. Ambient Pressure X-ray Photoelectron Spectroscopy. Ambient pressure XPS experiments were performed using the NAPP end station of the CIRCE beamline at the ALBA synchrotron radiation facility. The photon energy range at CIRCE is 100−2000 eV. The end station is equipped with a Phoibos NAP 150 electron energy analyzer. The analyzer is provided with four differentially pumped stages connected by small apertures. A set of electromagnetic lenses focuses the electrons though the apertures to maximize transmission. Such setup allows to keep the detector in ultrahigh vacuum (UHV) while the sample is at a maximum pressure of 20 mbar.[17−19] The total electron energy resolution in the experimental conditions used for the high-resolution spectra was better than 0.3 eV. Further details about the system can be found elsewhere.[20] The two pieces of LN z-cut sample were mounted in the same molybdenum sample holder showing opposite surfaces, together with the PPLN sample. While all measurements on LN z-cut samples were performed sequentially during the same series, LN y-cut surface measurements were performed separately in a different experiment. A gold foil was mounted in electrical contact with the samples in all cases to be used as reference. The temperature was monitored by a K-type thermocouple placed inside the sample holder next to the crystals. Water (LC-MS Ultra CHROMASOLV, Fluka Sigma-Aldrich) was used to dose water vapor, and it was previously degassed by freeze−pump−thaw cycles.

The sample holder with the crystals and the gold foil was introduced in the preparation chamber and annealed at 10^{-7} mbar and 300 °C for 1 h followed by a slow cool down overnight process in high-vacuum (HV) conditions. The Au $4f_{7/2}$ core level was measured for each photon energy used in the experiment, and its known binding energy (BE), BE (Au $4f_{7/2}$) = 84.0 eV was used for BE calibration. High-resolution XPS spectra for the Nb 3d, O 1s, N 1s, and C 1s core levels were measured with photon energies of 700 eV, using an energy step of 0.05 eV and pass energy of 20 eV. The fitting of all XPS spectra peaks was performed using the CasaXPS software with a combination of Gaussian/Lorentzian functions in the ratio of 30:70 after a Shirley subtraction.

In this work, two different series of XPS experiments exploring the composition of samples interface were performed sequentially: first the interface was explored after exposure to different water pressures from high vacuum to 4 mbar at room temperature (RT, 25 °C), then the pressure was reduced down to 2.5 mbar, and finally, the temperature was changed from RT up to 400 °C at a constant ambient water pressure of 2.5 mbar. Each spectrum, for all temperature and pressure conditions, was taken on a different fresh spot in order to minimize beam damage and average out local inhomogeneities of the sample. The interface behavior was approached by evaluating Nb 3d and O 1s XPS spectra. C 1s core level was also monitored during the experiment, and a small peak in the carbon region was found for all samples with a BE mainly corresponding to graphitic carbon (284.5 eV). However, the presence of C−O species cannot be excluded from our spectra[21] (see Figure S1). It is well-known that carbon contamination cannot be totally avoided in AP-XPS experiments when water vapor is introduced in the chamber, since beyond sample surface contamination, organic molecules are easily desorbed by the water vapor from different parts of the chamber, especially the sample holder, and deposited on the sample.[22]

3. RESULTS

3.1. Surface Discharge Dynamics. XPS measurements are based on the detection of sample-emitted electrons due to X-ray irradiation. Therefore, if the emitted electrons are not replaced, the sample charges relative to the instrument. This causes a retarding electric field at the sample surface and induces a loss in the kinetic energy of the emitted electrons, unless the field is compensated. If this effect is very strong, very few electrons reach the analyzer. This issue is particularly relevant in highly dielectric samples. This is the case for the ferroelectric single crystals used in this work, for which the loss of intensity due to the strong charging of the insulating substrate was so severe that it was not possible to obtain data for pressures below 0.5 mbar.

DOI: 10.1021/acs.jpcc.6b05465
J. Phys. Chem. C XXXX, XXX, XXX−XXX

Surface discharge of dielectric crystals under X-ray radiation can happen mainly through three different mechanisms: surface charge diffusion, discharge through the ionized gas in the case of AP-XPS, and bulk charge diffusion. The last channel is strongly limited in dielectric materials, and discharge through the ionized gas was proved to be also less relevant if compared to the surface charge diffusion by performing the same experiment in a N_2 environment instead of water, where the later mechanism is not present. Therefore, the study of surface discharge under X-ray radiation in different water atmospheres allows for the characterization of surface discharge dynamics by surface charge diffusion as a function of the polarization state and surface composition.

Figure 1a shows the kinetic energy (KE) from photoelectrons of Nb 3d core level measured on the positive LN z-cut face as a function of increasing water pressure. Similar spectra were obtained from the z-cut negative face and the y-cut crystal. The shift of the peaks (Nb 3d5/2 and Nb 3d3/2) to higher kinetic energies for increasing pressures indicates the progressive global discharge of the surface, after the initial charged state at low pressures. In addition, there is an attenuation of the peak intensity for increasing pressures due to the scattering of the electrons by collisions with the water and hydroxyl molecules adsorbed on the crystal and the water vapor molecules present in the chamber when the electrons travel through the gap between the surface and the analyzer entrance. The KE of the Nb 3d5/2 peak is plotted as a function of water pressure in Figure 1b for the three crystals: positive and negative LN z-cut and LN y-cut. For pressures above 2.5 mbar the KE shift is minimum and at 4 mbar the discharged state is achieved, with a BE of 207.3 eV, close to the value reported in the literature (207.2 eV).[14,23] Still, the discharge process following the evolution of the KE as a function of water pressure is found to be different for each surface. The peaks measured on the LN z-cut positive face show a slightly higher KE than the peaks measured on the LN z-cut negative surface for all water pressures below 4 mbar except for the lowest pressure of 0.5 mbar. KE at this pressure is found to be strongly dependent on the spot measured (see Figure S2). Moreover, the value of the KE peak increases at low water pressures and then stabilizes to a plateau in both LN z-cut surfaces up to 2 mbar, after which there is a progressive discharge evolution to the stable state. Instead, the KE peak position measured on the LN y-cut surface shows a strong increase for pressures below 1.5 mbar up to almost a completely discharged state, indicating a fast discharge of the surface at lower pressures than for the LN z-cut faces. The same measurements performed in N_2 atmosphere (see triangles in Figure 1b) showed an intense charging of the surface persisting up to 4 mbar of N_2 pressure, confirming the key role of surface discharge mechanism through the adsorbed water film for these materials.

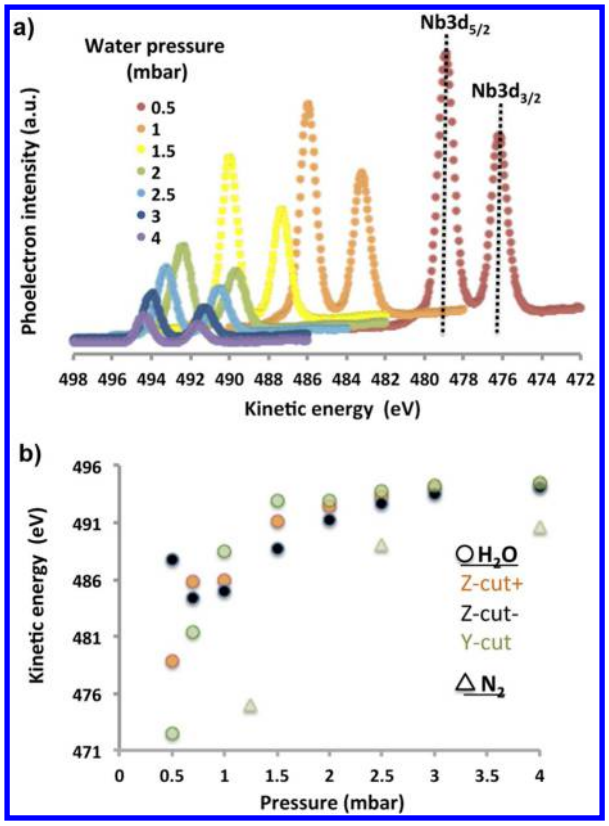

Figure 1. (a) Evolution of the Nb 3d electrons kinetic energy for a positive LN z-cut face as a function of increasing water pressure. (b) Kinetic energy corresponding to Nb 3d 5/2 electrons as a function of water vapor pressure, as measured on positive (z-cut+, orange circles) and negative (z-cut-, black circles) LN z-cut and LN y-cut (y-cut, green circles) surfaces. The evolution is also compared to the same measurements as a function of N_2 pressure on LN z-cut negative surface (gray triangles).

3.2. Water Adsorption on Polar Surfaces as a Function of Water Pressure. Figure 2a shows the XPS spectra in the O 1s region at room temperature for 2.5 mbar of water pressure, measured with a photon energy of 700 eV on the positive z-cut surface. The spectra were deconvoluted into five components: four surface contributions and a gas phase contribution. Due to the variable sample charging at the lowest pressures, the binding energies were varying slightly among different spectra. Therefore, the oxide peak was used to calibrate the energy in each case. The correct position of the BE peak at the lowest energy, corresponding to the oxides components, was fixed from spectra taken at noncharged samples, as indicated by the position of the Nb 3d peak (Figure 1), and calibrated using Au $4f_{7/2}$ as a reference. According to previously reported AP-XPS water adsorption experiments on MgO,[24] Cu,[25] and GaAs(100),[26] the following contributions to the O 1s core level can be expected (with BE extracted from GaAs(110)[26]): oxides (530.4 ± 0.1 eV), hydroxides (531.4 ± 0.1 eV), OH species H-bonded to H_2O molecules (531.8 ± 0.2 eV), and molecularly adsorbed water (532.5−533 eV). In addition, a gas phase H_2O peak can be observed at high pressures at around BE = 535 eV.

The fitting procedure was the following: as mentioned above, the oxide position was used as a reference, and therefore it was fixed to position x and the corresponding positions for the hydroxides OH and OH groups bonded to H_2O peaks were forced to remain at a constant distance of $(x + 1) \pm 0.2$ eV and $(x + 1.4) \pm 0.2$ eV, respectively. The presence of two −OH peaks is needed for a good fitting of all the spectra, and, at high temperature, where molecular water is desorbed from the surface, the existence of the hydroxides peak at $(x + 1) \pm 0.2$ eV is clearly observed (see Discussion below about temperature-dependent data). Finally, the fitting of the surface oxygen spectra is completed with a fourth peak corresponding to molecular H_2O free to move from $x + 2$ to $x + 2.5$ eV. OH and water peaks are very close in BE to peaks associated with C−O bonds.[27] Since some peaks associated with oxidized carbon, i.e.,

DOI: 10.1021/acs.jpcc.6b05465
J. Phys. Chem. C XXXX, XXX, XXX−XXX

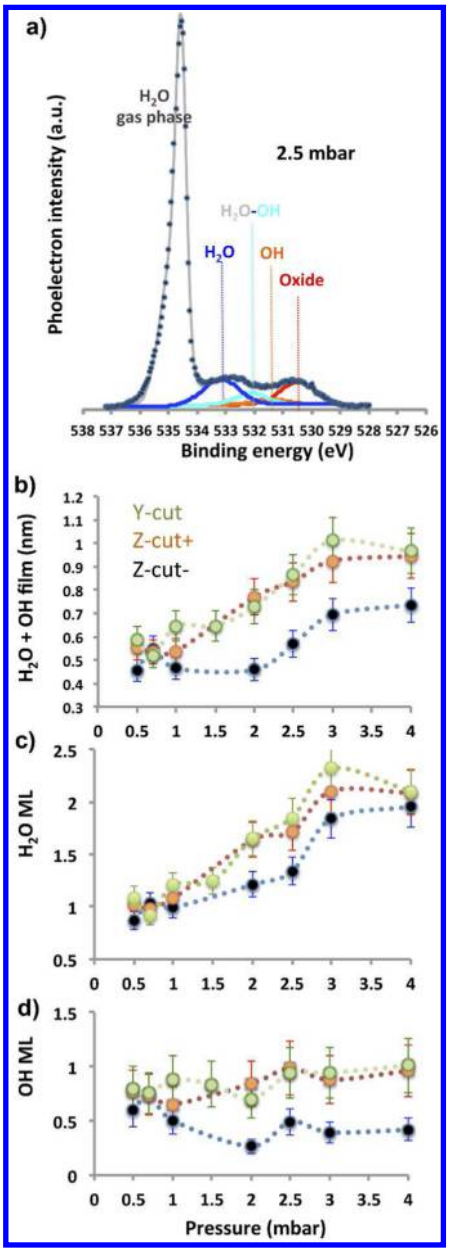

Figure 2. (a) XPS spectra in the O 1s region at room temperature at 2.5 mbar of water pressure on the positive z-cut surface with a photon energy of 700 eV. The mean feature is deconvoluted in five contributions: four surface contributions and a gas phase contribution at the highest BE. The peaks assignment from lower to higher BE is a peak corresponding to $LiNbO_3$ oxygen, two OH peaks, and molecular adsorbed water peak. (b) Total thickness of the adsorbates layer (H_2O + OH) as a function of water vapor pressure for positive LN z-cut, negative LN z-cut, and LN y-cut. (c) Water ML as a function of water vapor pressure for the three surfaces mentioned above. Water is found to absorb at lower pressures on LN y-cut and positive LN z-cut surfaces than on negative LN z-cut surface. (d) OH MLs on each surface as a function of water vapor pressure. The three surfaces show different evolutions; the OH intensity remains almost stable on LN y-cut surface, increase slightly on positive LN z-cut, and decreases on negative LN z-cut.

C═O and C−OH, are observed in the C 1s region spectra for the LN y-cut surface (see Figure S1), a possible additional contribution from organic molecules to the measured OH and water peaks must be considered.[21] These contributions have been subtracted using the methods described in the literature.[24,28]

To quantitatively analyze the amount of H_2O molecules and OH groups on the surfaces we followed procedures used by Newberg et al.[24] Using the intensity of the peaks associated with oxides, OH groups, and H_2O, the thickness of the adsorbed H_2O and OH films can be calculated as a function of water vapor pressure (Figure 2b). The model used takes into account the theoretical inelastic mean free path of electrons for an incident X-ray photon energy of 700 eV in water, OH, and oxides (λ_{H2O} = 1.17 nm, λ_{OH} = 0.91 nm, and λ_{Ox} = 7.67 nm) and the number of oxygen atoms per unit volume in each case (N_{H2O} = 33.4 atoms·nm^{-3}, N_{OH} = 48.9 atoms·nm^{-3}, N_{Ox} = 56.8 atoms·nm^{-3}). Electron inelastic mean free paths were calculated using the NIST Standard Reference Database 71 software v1.2.[24,29] Ab initio calculations have shown that LN z-cut positive and negative surfaces have a different termination surface with differences in the oxygen atoms density in the first three layers.[9] The same calculations showed that the LN y-cut surface could be interpreted as a sequence of $Li_2Nb_2O_6$ trilayers with a higher density of oxygen in the topmost layers. Taking these calculations into account, the surface oxygen density was determined experimentally by comparing the intensity of the Nb 3d5/2 peak and the O 1s peak associated with oxides: we obtained an O to Nb ratio of 3:1 for LN y-cut, 7:2 for positive LN z-cut, and 4:1 for negative LN z-cut. The same λ_{Ox} was used for each LN surface, but N_{Ox} was scaled from stoichiometric $LiNbO_3$ (N_{Ox} = 56.8) according to these ratios.

Figure 2b shows the thickness of the adsorbates film (water and OH groups) as a function of water vapor pressure. In all cases, there is an increase of the amount of adsorbates as the pressure increases from an initial state of 0.5 nm, with a clear step between 1 and 3 mbar. While this thickness monotonically increases with pressure for the positive z-cut and the y-cut surfaces from 1 mbar, a pressure of 2 mbar is needed to start observing changes on the thickness of adsorbates for the negative z-cut surface. Moreover, the amount of adsorbates at the highest pressure is not equivalent for all surfaces: while the LN y-cut and the positive LN z-cut crystal surface shows the highest content of adsorbed molecular water and OH groups with a thickness of 1 nm, this content is diminished for the negative LN z-cut surface, achieving a level of only 0.7 nm for the highest pressure.

The amount of water and OH groups (taken as the sum of the hydroxides and the OH species H-bonded to H_2O molecules) was plotted separately in Figure 2c and 2d in monolayers (ML) as a function of water pressure. Following the assumptions taken by Newberg et al., we defined the thickness of 1 ML of water as 0.31 nm[30] and 1 ML of OH according to its passivation thickness (0.31 nm in our case, as observed on positive LN z-cut and LN y-cut). Figure 2c shows that the initial state at the lowest pressure consisted of a ML of H_2O molecules for all surfaces, and this coverage rate is increased up to 2 ML at the highest pressure of 4 mbar for all of them, with slightly higher values for the LN z-cut positive surface with respect to the negative one. The trends, similar to the previous case, indicate that the onset of a second monolayer of coverage happens at lower pressures (1.5−2 mbar) for the y-cut and positive z-cut surfaces, while the step is only seen at 2.5−3 mbar for the negative z-cut surface. Finally, in Figure 2d it is observed that at 0.5 and 0.7 mbar the OH content scatters among half and full ML coverage for the three surfaces. From 1 to 4 mbar, the OH coverage values remain almost constant for

DOI: 10.1021/acs.jpcc.6b05465
J. Phys. Chem. C XXXX, XXX, XXX−XXX

LN y-cut surface and presents an antisymmetric behavior for LN z-cut surfaces with opposite polarization, with a clear step increase from 1 to 2 mbar for the positive z-cut surface, achieving a full ML coverage, and a decrease to less than half ML of coverage for the negative z-cut surface, indicating the least affinity of the negative surface to OH groups.

3.3. Water Desorption as a Function of Temperature.

In order to determine the strength of the interaction between the adsorbed water molecules as a function of the surface polarity, XPS spectra (shown in Figure 3) were recorded only

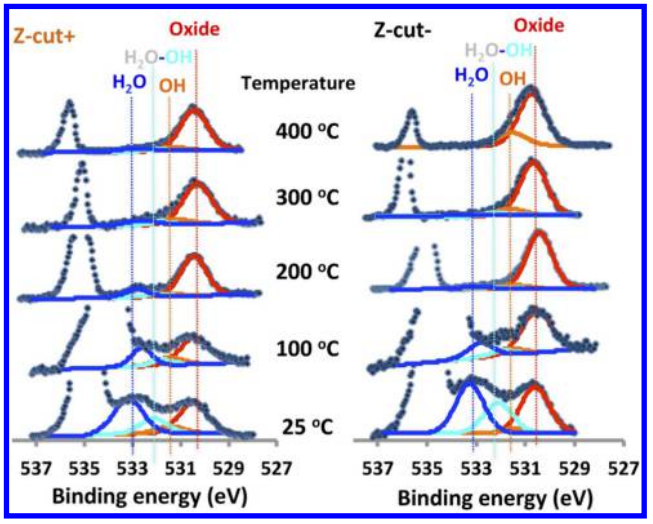

Figure 3. Evolution of the O1 s XPS spectra as a function of temperature at 2.5 mbar of water pressure for positive (left-hand side) and negative (right-hand side) LN z-cut surfaces.

for LN z-cut surfaces with opposite polarization as a function of increasing temperatures from RT up to 400 °C at a constant water vapor pressure of 2.5 mbar. This value of pressure was chosen as a compromise to minimize charging effects while keeping a good intensity of the peaks. The initial state was achieved after decreasing the pressure from 4 to 2.5 mbar. In this way, the initial state enclosed a similar amount of water molecules, above 2 ML for both surfaces, as shown in Figure 4a by RT measurements. Although this might seem to be incoherent with the data in Figure 2c and 2d, this is as a consequence of the well-known hysteretic behavior between adsorption and desorption of water when changing water vapor pressure or relative humidity; decreasing the pressure from 4 to 2.5 mbar did not show an important decrease in the amount of water on the two surfaces, and the coverage levels of 1.25 and 1.75 ML at 2.5 mbar shown in Figure 2c were not recovered. As in the previous series, spectra were taken for each temperature on both samples correlatively, thus undergoing exactly the same thermal treatment under the same experimental conditions.

Figure 3 shows the deconvolution of selected spectra taken on both polar surfaces as a function of temperature. The assignment of components for the XPS spectra analysis was done as explained in the previous section. At a first glance, thermal evolution of the spectra already shows how the peak assigned to molecular water adsorbed on the surface decreases as the temperature increases, with a faster rate for the negative LN z-cut face. For example, at 200 °C the H_2O peak practically disappears on the negative LN z-cut face, being still observable on the sample with positive polarization. This can be better observed in Figure 4a, where the thickness of adsorbed

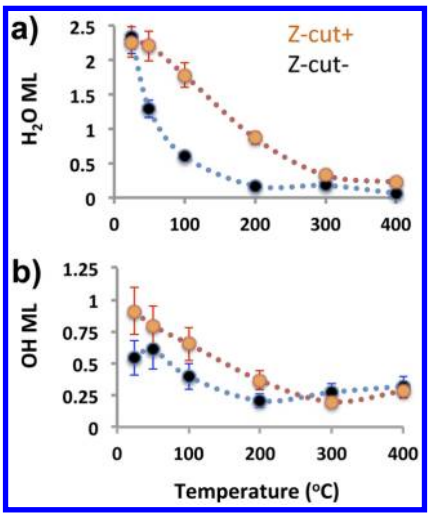

Figure 4. (a) Water ML and (b) OH MLs on each surface (see main text), as a function of temperature at 2.5 mbar of water vapor pressure. Water desorbs from the negative LN z-cut surface at lower temperatures than from the positive surface, as correlated with the higher presence of OH groups that play a predominant role in the strength of molecular water adsorption.

molecular water is plotted as a function of temperature for both samples. The negative LN z-cut surface shows a fast decrease of adsorbed water molecules between 2 ML RT down to almost 0 at 200 °C, while at positive LN z-cut surface water molecules are progressively released from the surface with increasing temperatures up to more than 300 °C. Thickness of the OH groups is shown in Figure 4b. The initial coverage state is lower for the negative z-cut surface, and shows a small peak below 100 °C followed by a decay of the OH thickness to a minimum value of a quarter monolayer above 200 °C, while the positive z-cut surface shows a monotonic decrease from room temperature down to 300 °C, where it stabilized in the same minimum value of a quarter monolayer. Similar to H_2O molecules, this decay happens at lower temperatures for the negative z-cut surface. For temperatures above 300 °C the intensity seems to remain constant with a stable permanent coverage of a quarter monolayer. Different studies[31,32] indicate that the surface on LN does not undergo reconstruction until annealed at higher temperatures, i.e., above 600 °C, when all the adsorbates are removed from the surface so we can assume that the stoichiometry of the surface of the crystal is stable in our temperature range.

4. DISCUSSION

Our ambient pressure x-ray photoelectron spectroscopy experiments demonstrate the polarization-dependent water adsorption on the different faces of $LiNbO_3$ single crystals, as previously suggested from ab initio calculations[15] and temperature-programed desorption (TPD) experiments.[13] As expected from ab initio calculations, molecular adsorption was found to be favored over dissociative adsorption, but dissociative adsorption was also observed, perhaps induced by the presence of defects, other adsorbates, or specially stray fields of ferroelectric surfaces not considered in the calculations. In our experiments, peaks associated with OH groups are found in all spectra, and a reasonable good fitting of the spectra without taking into account the presence of these peaks is not possible. It is also confirmed by the presence of a remaining quarter ML of OH groups at the highest measured temperatures when all

DOI: 10.1021/acs.jpcc.6b05465
J. Phys. Chem. C XXXX, XXX, XXX−XXX

molecular water is removed, supporting the inclusion of OH peaks in all conditions. Still, to have more insight in the mechanisms of formation of the OH groups it would be necessary to obtain data at lower pressures, which in this case is prevented due to strong charging effects.

Our experiments show the formation of a second H_2O ML on all surfaces as pressure changes from 1 to 3 mbar, at a slower rate for the negative z-cut surface. This behavior is consistent with the predicted phase transition from low to high coverage structures in calculated phase diagrams from ab initio calculations, taking into account only nondissociative adsorption.[15] These calculations suggested that at RT and near ambient pressures, the surface would be covered by single molecules (on the LN z-cut positive face) or hexagonal films (on the LN z-cut negative face) for a sub-ML and a ML coverage regime. At a high coverage degree, 3D icelike structures were suggested for both LN z-cut faces. According to this calculated phase diagram, the high-coverage regime should be reached between 5 to 30 mbar of pressure, while our experiments indicate a transition from a 1 ML of water coverage to a 2 ML state between 1 and 3 mbar for all surfaces. In this sense, differences between the experimental and calculated pressures at which the transition takes place could be explained by taking into account the presence of OH species as observed in our measurements, which would certainly modify the phase diagram. On the other hand, the LN y-cut surface shows a similar trend of a phase transition from the ML coverage to the high-coverage regime at pressures between 1.5 and 2 mbar, and even to the best of our knowledge, there is no calculation of water adsorption on this LN face with which to compare. At a pressure of 1 mbar, the nonpolar LN y-cut surface already shows high values of OH groups close to its stable content, while the polar LN z-cut surfaces seem to show lower content of OH groups. This might be explained by the occurrence of different water dissociation processes in polar and nonpolar surfaces, favoring the creation of OH groups in nonpolar surfaces, or by the enhancement of recombination processes of OH groups with the polar surfaces as compared with the nonpolar ones at low coverage rates.

Even all the LN surfaces show the same phase transition between 1 and 2 ML of H_2O, the total thickness of the adsorbates film (including both H_2O molecules and OH groups) differs significantly from LN y-cut or positive z-cut surfaces and negative z-cut surface, showing the presence of higher thickness of adsorbates films for the first group at high pressures.

The formation of a second H_2O ML in all surfaces is shown to be strongly related to the trigger of surface conductivity as observed by two facts: the onset of diffusion of ionic OH species that play a role in the screening mechanisms of the depolarizing ferroelectric surface fields and the onset of general surface discharge observed in Figure 1b at the same pressures at which the second ML of H_2O starts to adsorb.

The first point is consistent with the onset of the divergence of OH groups' thickness on opposite polarized z-cut surfaces at a pressure of 1 mbar, which we ascribe to an enhancement of the OH groups mobility that favors the migration of OH groups along the surface. The relationship between water and OH groups on the surface of positive and negative LN z-cut as a function of water pressure is schematically drawn in Figure 5. Once the second H_2O ML is formed, the main role of the OH groups is associated with the screening of ferroelectric depolarizing fields, and thus LN z-cut negative surface is less

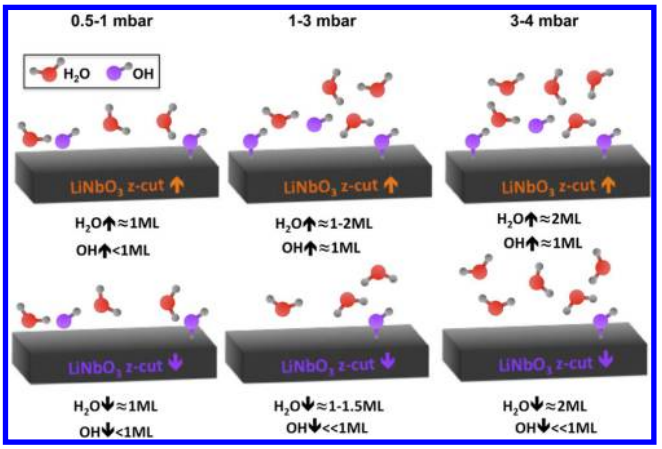

Figure 5. Schematics summarizing the differences on water molecules and OH groups' presence on the positive and negative LN z-cut surfaces as a function of water vapor pressures. This scheme does not intend to represent a realistic model of the adsorption geometry of OH or water molecules on the surface.

favorable to the presence of these negatively charged groups and more prone to retain their counterparts, that is, protonic H^+ ions (not observable by XPS). Still, LN z-cut positive surface does not seem to increase the OH group content beyond the nonpolar surface, indicating that the surface polarity is not determinant for water dissociation processes. In this case, we can assume that surface charge screening is achieved by a reduction of protonic H^+ ions, assisted by surface diffusion processes. Adsorption of both H^+ and OH on positive and negative LN surfaces has been studied using ab initio calculations.[15] Results showed that the absorption is favored for OH at the negative face and for H at the positive face. Still, it has to be taken into account that experimental and calculation conditions are not directly comparable in this respect, and not necessarily contradictory.

Measurements of water and OH intensity as a function of water vapor pressure performed on a PPLN surface showed that this surface shows a trend in between the negative z-cut LN surface and the positive one (see Figure S3).

Desorption experiments performed at 2.5 mbar of water pressure also indicate a stronger water affinity at the positive LN z-cut surface, with the presence of adsorbed water molecules up to 300 °C, as compared to the negative surface, where complete water desorption is already observed at 200 °C. TPD results by Garra et al.[13] in UHV conditions showed the same trend in positively and negatively polarized LN z-cut surfaces. Notice that peaks related to molecular water have also been observed at temperatures as high as 300 °C using AP-XPS on other surfaces such as GaAs(100)[26] in ambient conditions, in which dissociation of water and formation of surface OH was also observed. According to that, and taking into account the results shown in Figure 4b, OH groups might help anchor the water molecules to the surface, which might be more strongly bounded to the positive LN z-cut surface than to the negative one mainly due to the major presence of OH groups, rather than by their dipolar interaction with the polarization of the surface. In this sense, the lack of OH groups in negative z-cut surfaces at a pressure around 2 mbar due to the onset of surface charge mobility and screening activity (they might be repelled by depolarizing field on this surface) can also influence the ability of that surface to retain water molecules and thus delay

DOI: 10.1021/acs.jpcc.6b05465
J. Phys. Chem. C XXXX, XXX, XXX−XXX

the formation of the second H_2O ML on z-cut negative surfaces to higher pressures.

Our work demonstrates how surface charging, a common hindrance in photoemission experiments on insulating samples, can be used in AP-XPS to obtain information about surface conductivity induced by adsorbed species. In previous studies, the shift of the position of the Na 1s and Cl 2p peaks in a NaCl crystals due to sample charging in AP-XPS measurements has been directly related to the amount of water molecules adsorbed on the surface.[33] In that case, the adsorption of water induced the dissolution of ions at the surface and the discharge of the surface through the surface ionic mobility. Surface discharging through the water layer adsorbed on the surface has also been observed on oxide samples using AFM; for example, the discharge of graphene layers on silicon oxide[34] or surface screening of polar domains created in a PZT thin film have been reported.[35] As mentioned before, electrons created during XPS measurements leave uncompensated charges at the sample. The sample can discharge through the bulk of the crystal, through the gas phase in contact with the sample, and through the water layer adsorbed on the surface. Discharging through the bulk should be constant during the experiment and almost negligible in the case of high dielectric materials such as ferroelectric single crystals, while discharging through the gas and the water adsorbed on the surface will increase as the water vapor in the chamber is increased. Minor discharging through the water vapor atmosphere is still present, as observed by comparison with discharging processes when using another gas such as N_2. Thus, surface discharging is expected to happen mainly by the mobility of the ionic species created from water dissociation (H^+ and OH^-) through the second surface water layer, as confirmed by the correlation of the onset of the shift of the Nb 3d peak (Figure 1b) with the formation of the second H_2O ML, as shown in Figure 2c. Similar surface charging trends, not shown here, were observed for the data obtained as a function of temperature, with increased charging effects correlated with the decrease of surface water content. This charging effect has been corrected to show the real BE of spectra shown in Figure 3.

It is important to remember that the onset of mobility of ionic species through the second H_2O ML allows the activation of surface screening mechanisms on polarized surfaces; OH groups, charged negatively, will screen the positive surface, while on the negative surface OH groups are expected to migrate through the water layer to allow screening of the negative polarization surface charge, and thus a decrease on OH thickness is expected as observed in Figure 2d. The direct correlation of mobility of ionic species with water content is further confirmed by the fast discharge process of LN y-cut surface, for which the complete formation of the second water ML is achieved at the lowest pressure. Finally, although it is out of the scope of the experimental results, it cannot be excluded that the slight differences in the observed discharge processes might be correlated with intrinsic difference in the mobility of the known surface ionic species as a function of the LN face, and the corresponding adsorbed water structure. However, in our experiments the ionic mobility seems to be independent of the surface and therefore only associates with the surface water thickness.

5. CONCLUSIONS

In this work, AP-XPS was used to study the interface of LN ($LiNbO_3$) surfaces exposed to water vapor at different pressure and temperature conditions. The O 1s spectra indicate the presence of additional components that are associated with different OH groups at the surface, giving evidence of partial dissociation of water molecules at the surfaces, although the exact mechanisms of formation of these OH groups could not be clearly determined.

We compared directly positive and negative LN z-cut surfaces (with polarization pointing up and down respectively) with nominally nonpolar LN y-cut surface, observing a preferential adsorption on the nonpolar and positive surface vs the negative surface, with a general transition from 1 ML to 2 ML of H_2O coverage state at water pressures between 1.5 and 2 mbar for the positive z-cut polar surface, and between 2.5 and 3 mbar for the negative z-cut polar surface. The highest thickness of water molecules at the surface for the LN y-cut surface, and LN z-cut positive surface, can be directly correlated with the presence of OH groups on the surface, which seem to play a predominant role for water molecules adsorption beyond the dipolar electric interactions due to polarization states of the surface. Surface ionic mobility is observed to be strongly correlated with the presence of the second water ML, which seems to trigger both general surface discharge and adsorbates screening effects. The stronger affinity of water for the polar LN z-cut positive surface as compared to the negative surface in the high coverage regime is also consistent with the higher presence of OH groups; negative OH charged groups are expelled from the LN z-cut negative surface once the ionic mobility on the surface is guaranteed by the formation of the second water ML. This stronger bonding persists as a function of temperature and is coherent with the observed enhanced desorption temperature for the positive LN z-cut surface at 300 °C, in contrast with the total desorption at 200 °C observed for the negative LN z-cut surface. Again, OH groups show a preferential role in water adsorption as a function of temperature, and a stable submonolayer of OH groups is observed to persist on the surface at 400 °C for all surfaces, when all water molecules are completely desorbed.

Finally, the main mechanism of surface discharge is observed to happen through the ionic mobility along the adsorbed water layer. In this sense, mobility of the known surface ionic species seems to be mainly determined by the formation of a second water monolayer and seems to be almost independent of surface polarization.

■ ASSOCIATED CONTENT

Supporting Information

The Supporting Information is available free of charge on the ACS Publications website at DOI: 10.1021/acs.jpcc.6b05465.

C 1s spectra for positive and negative LN z-cut and LN y-cut surfaces (Figure S1); Nb peak discharge for two different spots of the same sample (Figure S2); water and OH as a function of pressure on a PPLN surface (Figure S3) (PDF)

■ AUTHOR INFORMATION

Corresponding Authors

*E-mail: neus.domingo@icn2.cat. Tel.: +34 93 737 3617.
*E-mail: averdaguer@icn2.cat. Tel.: +34 93 737 1601.

Notes

The authors declare no competing financial interest.

DOI: 10.1021/acs.jpcc.6b05465
J. Phys. Chem. C XXXX, XXX, XXX−XXX

■ ACKNOWLEDGMENTS

This work has been partially funded by the 2014 SGR 1216 project from the Generalitat de Catalunya, the MAT2012-38319-C02-01, the FIS2013-48668-C2-1-P, and FIS2015-73932-JIN from the Spanish Ministerio de Economía y Competitividad (MINECO). K.C-E.'s work was funded by an ERC Starting Grant from the EU (Project No. 308023). N.D. is also grateful to MINECO for the "Ramon y Cajal" contract RYC-2010-06365. ICN2 acknowledges support from the Severo Ochoa Program (MINECO, Grant SEV-2013-0295). The authors want to thank Dr. J. Zapata for his assistance in graphics design.

■ REFERENCES

(1) Scott, J. F. *Ferroelectric Memories*; Springer: Berlin, New York, 2000; p xvi, 248 pp.
(2) Tybell, T.; Ahn, C. H.; Triscone, J. M. Ferroelectricity in Thin Perovskite Films. *Appl. Phys. Lett.* **1999**, *75*, 856−858.
(3) Kalinin, S. V.; Bonnell, D. A. Temperature Dependence of Polarization and Charge Dynamics on the BaTiO3(100) Surface by Scanning Probe Microscopy. *Appl. Phys. Lett.* **2001**, *78*, 1116−1118.
(4) Peter, F.; Szot, K.; Waser, R.; Reichenberg, B.; Tiedke, S.; Szade, J. Piezoresponse in the Light of Surface Adsorbates: Relevance of Defined Surface Conditions for Perovskite Materials. *Appl. Phys. Lett.* **2004**, *85*, 2896−2898.
(5) Li, D. B.; Zhao, M. H.; Garra, J.; Kolpak, A. M.; Rappe, A. M.; Bonnell, D. A.; Vohs, J. M. Direct in Situ Determination of the Polarization Dependence of Physisorption on Ferroelectric Surfaces. *Nat. Mater.* **2008**, *7*, 473−477.
(6) Yun, Y.; Altman, E. I. Using Ferroelectric Poling to Change Adsorption on Oxide Surfaces. *J. Am. Chem. Soc.* **2007**, *129*, 15684−15689.
(7) Rode, S.; Holscher, R.; Sanna, S.; Klassen, S.; Kobayashi, K.; Yamada, H.; Schmidt, W. G.; Kuhnle, A. Atomic-Resolution Imaging of the Polar (0001) Surface of $LiNbO_3$ in Aqueous Solution by Frequency Modulation Atomic Force Microscopy. *Phys. Rev. B: Condens. Matter Mater. Phys.* **2012**, *86*, 075468.
(8) Gui, L.; Hu, H.; Garcia-Granda, M.; Sohler, W. Local Periodic Poling of Ridges and Ridge Waveguides on X- and Y-Cut $LiNbO_3$ and Its Application for Second Harmonic Generation. *Opt. Express* **2009**, *17*, 3923−3928.
(9) Sanna, S.; Schmidt, W. G. Lithium Niobate X-Cut, Y-Cut, and Z-Cut Surfaces from ab Initio Theory. *Phys. Rev. B: Condens. Matter Mater. Phys.* **2010**, *81*, 214116.
(10) Berth, G.; Wiedemeier, V.; Husch, K. P.; Gui, L.; Hu, H.; Sohler, W.; Zrenner, A. Imaging of Ferroelectric Micro-Domains in X-Cut Lithium Niobate by Confocal Second Harmonic Microscopy. *Ferroelectrics* **2009**, *389*, 132−141.
(11) Soergel, E. Piezoresponse Force Microscopy (PFM). *J. Phys. D: Appl. Phys.* **2011**, *44*, 464003.
(12) Tanzilli, S.; Tittel, W.; De Riedmatten, H.; Zbinden, H.; Baldi, P.; De Micheli, M.; Ostrowsky, D. B.; Gisin, N. Ppln Waveguide for Quantum Communication. *Eur. Phys. J. D* **2002**, *18*, 155−160.
(13) Garra, J.; Vohs, J. M.; Bonnell, D. A. The Effect of Ferroelectric Polarization on the Interaction of Water and Methanol with the Surface of $LiNbO_3$(0001). *Surf. Sci.* **2009**, *603*, 1106−1114.
(14) Herdiech, M. W.; Monig, H.; Altman, E. I. An X-ray Photoelectron Spectroscopy Study of Bf3 Adsorption on Positively and Negatively Poled $LiNbO_3$(0001). *Surf. Sci.* **2014**, *626*, 53−60.
(15) Sanna, S.; Holscher, R.; Schmidt, W. G. Polarization-Dependent Water Adsorption on the $LiNbO_3$(0001) Surface. *Phys. Rev. B: Condens. Matter Mater. Phys.* **2012**, *86*, 205407.
(16) Holscher, R.; Schmidt, W. G.; Sanna, S. Modeling $LiNbO_3$ Surfaces at Ambient Conditions. *J. Phys. Chem. C* **2014**, *118*, 10213−10220.
(17) Ogletree, D. F.; Bluhm, H.; Lebedev, G.; Fadley, C. S.; Hussain, Z.; Salmeron, M. A Differentially Pumped Electrostatic Lens System for Photoemission Studies in the Millibar Range. *Rev. Sci. Instrum.* **2002**, *73*, 3872−3877.
(18) Bluhm, H. Photoelectron Spectroscopy of Surfaces under Humid Conditions. *J. Electron Spectrosc. Relat. Phenom.* **2010**, *177*, 71−84.
(19) Starr, D. E.; Liu, Z.; Havecker, M.; Knop-Gericke, A.; Bluhm, H. Investigation of Solid/Vapor Interfaces Using Ambient Pressure X-ray Photoelectron Spectroscopy. *Chem. Soc. Rev.* **2013**, *42*, 5833−5857.
(20) Perez-Dieste, V.; Aballe, L.; Ferrer, S.; Nicolas, J.; Escudero, C.; Milan, A.; Pellegrin, E. Near Ambient Pressure XPS at Alba. *J. Phys.: Conf. Ser.* **2013**, *425*, 072023.
(21) Iliut, M.; Leordean, C.; Canpean, V.; Teodorescu, C. M.; Astilean, S. A New Green, Ascorbic Acid-Assisted Method for Versatile Synthesis of Au-Graphene Hybrids as Efficient Surface-Enhanced Raman Scattering Platforms. *J. Mater. Chem. C* **2013**, *1*, 4094−4104.
(22) Verdaguer, A.; Weis, C.; Oncins, G.; Ketteler, G.; Bluhm, H.; Salmeron, M. Growth and Structure of Water on SiO_2 Films on Si Investigated by Kelvin Probe Microscopy and in Situ X-Ray Spectroscopies. *Langmuir* **2007**, *23*, 9699−9703.
(23) Yun, Y.; Pilet, N.; Schwarz, U. D.; Altman, E. I. Comparison of the Interaction of Pd with Positively and Negatively Poled $LiNbO_3$(0001). *Surf. Sci.* **2009**, *603*, 3145−3154.
(24) Newberg, J. T.; et al. Formation of Hydroxyl and Water Layers on MgO Films Studied with Ambient Pressure XPS. *Surf. Sci.* **2011**, *605*, 89−94.
(25) Andersson, K.; Ketteler, G.; Bluhm, H.; Yamamoto, S.; Ogasawara, H.; Pettersson, L. G. M.; Salmeron, M.; Nilsson, A. Bridging the Pressure Gap in Water and Hydroxyl Chemistry on Metal Surfaces: The Cu(110) Case. *J. Phys. Chem. C* **2007**, *111*, 14493−14499.
(26) Zhang, X. Q.; Ptasinska, S. Dissociative Adsorption of Water on an H_2O/GaAs(100) Interface: In Situ Near-Ambient Pressure XPS Studies. *J. Phys. Chem. C* **2014**, *118*, 4259−4266.
(27) Pintilie, L.; Ghica, C.; Teodorescu, C.; Pintilie, I.; Chirila, L.; Pasuk, J.; Trupina, L.; Hrib, L.; Boni, A.; Apostol, N.; Abramiuc, L.; Negrea, R.; Stefan, M.; Ghica, D.; et al. Polarization Induced Self-Doping in Epitaxial Pb(Zr0.20Ti0.80)O−3 Thin Films. *Sci. Rep.* **2015**, *5*, 149740.
(28) McCafferty, E.; Wightman, J. P. Determination of the Concentration of Surface Hydroxyl Groups on Metal Oxide Films by a Quantitative XPS Method. *Surf. Interface Anal.* **1998**, *26*, 549−564.
(29) Powell, C. J.; Jablonski, A.; Salvat, F. Nist Databases with Electron Elastic-Scattering Cross Sections, Inelastic Mean Free Paths, and Effective Attenuation Lengths. *Surf. Interface Anal.* **2005**, *37*, 1068−1071.
(30) Ewing, G. E. Ambient Thin Film Water on Insulator Surfaces. *Chem. Rev.* **2006**, *106*, 1511−1526.
(31) Sanna, S.; Rode, S.; Holscher, R.; Klassen, S.; Marutschke, C.; Kobayashi, K.; Yamada, H.; Schmidt, W. G.; Kuhnle, A. Charge Compensation by Long-Period Reconstruction in Strongly Polar Lithium Niobate Surfaces. *Phys. Rev. B: Condens. Matter Mater. Phys.* **2013**, *88*, 115422.
(32) Sanna, S.; Holscher, R.; Schmidt, W. G. Temperature Dependent $LINBO_3$(0001): Surface Reconstruction and Surface Charge. *Appl. Surf. Sci.* **2014**, *301*, 70−78.
(33) Verdaguer, A.; Segura, J. J.; Fraxedas, J.; Bluhm, H.; Salmeron, M. Correlation between Charge State of Insulating NaCl Surfaces and Ionic Mobility Induced by Water Adsorption: A Combined Ambient Pressure X-ray Photoelectron Spectroscopy and Scanning Force Microscopy Study. *J. Phys. Chem. C* **2008**, *112*, 16898−16901.
(34) Verdaguer, A.; Cardellach, M.; Segura, J. J.; Sacha, G. M.; Moser, J.; Zdrojek, M.; Bachtold, A.; Fraxedas, J. Charging and Discharging of Graphene in Ambient Conditions Studied with Scanning Probe Microscopy. *Appl. Phys. Lett.* **2009**, *94*, 233105.
(35) Segura, J. J.; Domingo, N.; Fraxedas, J.; Verdaguer, A. Surface Screening of Written Ferroelectric Domains in Ambient Conditions. *J. Appl. Phys.* **2013**, *113*, 187213.

DOI: 10.1021/acs.jpcc.6b05465
J. Phys. Chem. C XXXX, XXX, XXX−XXX